Electroluminescence characterization of mid-infrared InAsSb/AlInAs multi-quantum well light emitting diodes heteroepitaxially integrated on GaAs and Silicon wafers

A.R Altayar[1,3], F. A. Al-Saymari[1,4], E. Repiso[1], L. Hanks[1], A. P. Craig[1], M. Bentley[2], E. Delli[2], P. J. Carrington[2], A. Krier[1] and A.R. J. Marshall[1*].

[1]Department of Physics, Lancaster University, Bailrigg LA1 4YB, U.K.

[2]Department of Engineering, Lancaster University, Bailrigg, Lancaster, LA1 4YW, UK

[3]Department of Physics, College of Science, Al Imam Mohammad Ibn Saud University (IMISU), Riyadh, 11623, Saudi Arabia

[4]Department of Physics, College of Education for Pure Science, University of Basra, Basra, Iraq

[*] Corresponding author e-mail: a.r.marshall@lancaster.ac.uk

Abstract

Heteroepitaxy of mid-infrared Sb-based III-V semiconductor devices on highly mismatched wafers such as GaAs and silicon are a promising route towards high-density integration benefiting from the mature fabrication technology of these substrates. This work reports on the electrical performance of heteroepitaxially grown mid-infrared $InAs_{0.915}Sb_{0.085}/Al_{0.12}In_{0.88}As$ multi-quantum wells light emitting diodes on GaAs and offcut Si substrates using molecular beam epitaxy. Both devices exhibited a strong room temperature electroluminescence signal peaking at around 3.4 μm. Analysis of the output power results obtained from both devices revealed that the Si-based LED exhibited higher external quantum efficiency despite the higher defect density which is attributed to the superior thermal properties of the Si wafer.

Key words: A3. Molecular Beam Epitaxy, B3. Infrared Devices, B3. Light Emitting Diodes, B2. Semiconducting III-V materials, B1. Antimonides, A3. Quantum wells

1. Introduction

Photonic components operating in the mid-infrared (MIR) spectral region from 2 to 12 μm, are of increasing technological interest due to the potential applications in a vast variety of fields such as thermal imaging, absorption spectroscopy and medical diagnostics. Of these, MIR emitting devices such as light emitting diodes (LEDs) and lasers are of great interest for sensing applications, including monitoring of atmospheric pollutants, chemical processing control and detection of biological makers in non-invasive medical diagnostics, in addition to their potential in free-space optical communications[1–3]. Notably, much effort has been focused towards the development of LED devices operating at particular MIR wavelength regions depending on the specific detection applications [4,5]. This is due to the fact that several atmospheric gases, such as CH_4, CO_2 and CO, and biomolecules have their fundamental absorption bands in this spectral range. Particularly, Parry et al developed As-based bulk LED devices operating at 3.3 μm at room temperature promising for methane detection systems[4]. MIR LEDs are also considered as a far more attractive and cost-effective alternative to lasers especially for widespread distributed sensing applications which require many point sensors, portable instruments and low power consumption. To date, a wide range of homoepitaxial Sb-based III-V semiconductor devices have been developed [6–9] based on several quantum systems such as GaInAsSb/AlGaAsSb quantum wells (QWs) [9], InSb/InAs quantum dots (QDs) [10] and type-II InAs/GaSb superlattices (SLs) [11] demonstrating promising performance. More recently, significant progress has been made in the development of interband cascade LEDs (ICLEDs) exhibiting strong output power up to 1.4 mW and 0.5 mW at 4.2 and 4.7 μm respectively [12,13].

Development of mid-infrared III-V semiconductors LEDs on more mature substrates such as GaAs and silicon (Si) is increasingly being demonstrated benefiting from the pre-existing manufacturing technology, the availability of large size wafers and lower fabrication costs. Most importantly, direct growth on Si also provides the possibility of developing a complete MIR Si photonics platform for future integrated sensor circuits[14]. Recently, we reported on the optical properties of $InAs_{1-x}Sb_x/Al_yIn_{1-y}As$ QWs grown on GaAs via a relaxed AlInAs metamorphic buffer layer [15]. This material system is characterized by its unique ability to engineer compressively strained QWs which demonstrate a type-I band alignment with strong electron/hole wavefunction overlap. In this work, we report on bright electroluminescence obtained from type-I $InAs_{1-x}Sb_x/Al_yIn_{1-y}As$ multi-quantum wells (MQWs) LEDs grown on

GaAs and Si substrates and investigate the temperature and current-dependent properties of the devices.

2. Experimental Procedures

The samples were grown using a solid source Veeco GENxplor Molecular Beam Epitaxy (MBE) system. Valved cracker cells were used to provide arsenic (As) and antimony (Sb) fluxes and SUMO® cells are used to provide the In, Ga and Al-fluxes. During growth, the surface reconstruction was monitored using reflection high energy electron diffraction (RHEED). Two LEDs structures were grown using a 2µm-thick n-type $Al_{0.12}In_{0.88}As$ buffer layer, one on a 4 deg offcut toward [0-11] Si and one on a GaAs substrate, as shown in Figure 1. The growth of a high crystalline quality AlInAs buffer layer faces difficulties related to the large lattice mismatch to the wafers leading to the generation of misfit defects and threading dislocations. Furthermore, the large difference between the Al and In sticking coefficients leads to segregation and intermixing. Therefore, an optimized growth technique was used to grow the AlInAs buffer layer for each sample. For the GaAs-based structure, the growth temperature was reduced to 475˚C under an As flux following the growth of the GaAs buffer layer. The AlInAs buffer was deposited using a V/III flux ratio of 9 and a growth rate of 1µm/hr. Interfacial misfit (IMF) dislocations were generated at the InAlAs/GaAs interface to help release the misfit strain leading to a dislocation density of $\sim 1\times10^{9}cm^{-2}$. For the Si-based structure, a GaSb intermediate buffer layer was used between the Si and AlInAs buffer. This was grown using an AlSb IMF array and a two-step growth temperature technique (490 to 515 ˚C) to provide an antiphase domain (APD) free epilayer on Si with a smooth surface. Details of the Si wafer cleaning technique, the growth of the GaSb buffer layer and the surface characterization have been described previously[16,17]. Next the growth temperature was reduced to 475˚C under an Sb flux and a monolayer of Al was deposited on the GaSb buffer. AlInAs was then grown following the procedure described previously. Even though the surface dislocation density on the GaSb/Si buffer was expected to be low ($\sim10^{8}cm^{-2}$), the tensile strain at the InAlAs/GaSb interface was not successfully accommodated resulting in a high dislocation density of the order of $\sim 1\times10^{10}cm^{-2}$. Next, the same active region was deposited on top of each buffer structure grown comprising five periods of $InAs_{1-x}Sb_x/Al_xIn_{1-x}As$ MQWs with an Sb content of 8.5% in the InAsSb layers. The thickness of the $InAs_{0.91}Sb_{0.085}$ QWs and $Al_{0.12}In_{0.88}As$ barriers were 10 nm and 17 nm respectively. An optimized shutter sequence consisting of 10 seconds of As flux prior and 180 seconds following the growth of the InAsSb

QW were used to reduce the Sb and Al atoms segregation and improve the interface abruptness. The active region was grown using a growth temperature of 440 ˚C. The QWs were designed to exhibit a peak emission near $\lambda = 3.3$ µm at room temperature. Finally, an undoped 30nm $Al_{0.24}In_{0.76}As$ electron blocking barrier (EBL) was grown on the top of the active region and a 500nm-thick p-type $Al_{0.12}In_{0.88}As$ capping layer was deposited to finalize the structures.

The grown samples were processed into square 800µm × 800µm mesa-etch LEDs using photolithography and wet chemical etching process. The p-type AlInAs layers and MQW layers were etched using sulfuric acid: H_2O_2: H_2O (1:8:80). A 200 nm thick top metallic Ti/Au contact was deposited on the top of the p-type AlInAs layer by thermal evaporation and metal lift-off. A second photolithography step was carried out to pattern the sample for the subsequent wet etching of the mesa requiring etching through the structure and stopping within the n-AlInAs layer. Finally, a Ti/Au metallic contact was deposited on the n-AlInAs layer to provide an Ohmic contact to the n-side of the heterostructure. The electroluminescence (EL) signal was measured using a Bruker Vertex 70 Fourier transform infrared (FTIR) spectrometer. The system was connected to a temperature-controlled Oxford Instruments continuous flow helium cryostat enabling accurate controlling of the temperature within the sample chamber. A molecular sieve drying column was used to filter out atmospheric H_2O from the optical path. The output power of the prototype LEDs devices was measured at room temperature using an integrating sphere and a calibrated PbSe photodetector. The structural quality of both samples was characterized by high resolution x-ray diffraction (HRXRD) measurements using a Bede QC200 diffractometer. Bede Mercury RADS simulation software was used to determine the layer thickness and Sb content.

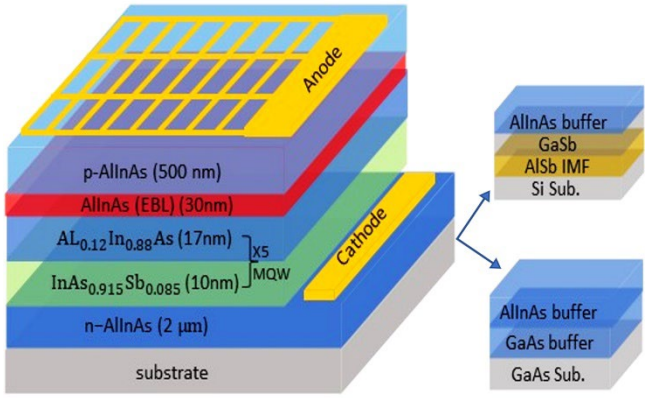

Figure 1: A schematic diagram of the InAsSb/AlInAs MQW LED grown on both GaAs and Si substrates.

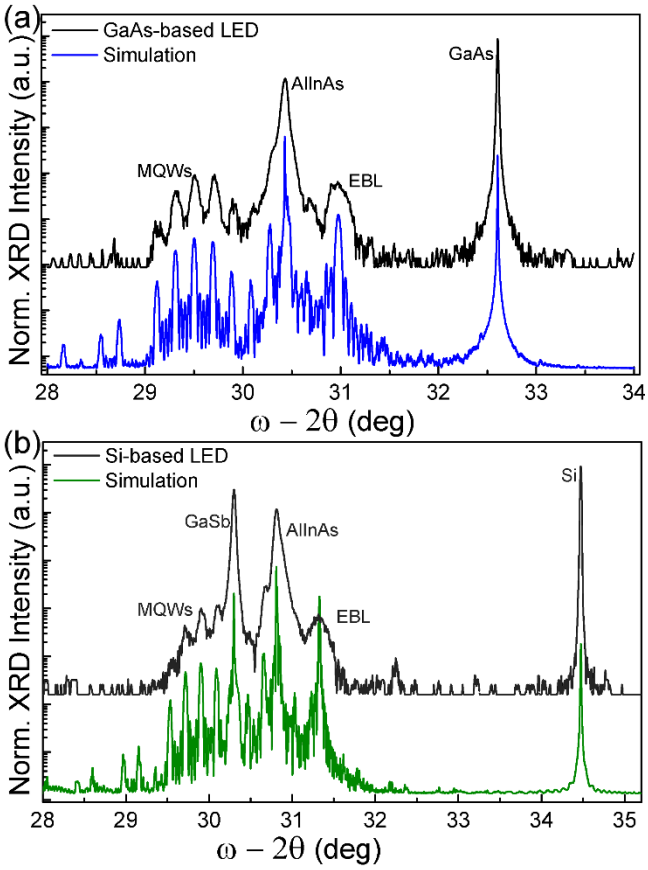

Figure 2: Experimental and simulated high resolution X-ray diffraction pattern of InAsSb/AlInAs MQW LEDs grown on a. GaAs and b. Si.

3. Results and discussion

The X-ray diffraction ω-2θ rocking curves obtained for the two InAsSb/AlInAs MQW LED samples are shown in Figure 2. RADS Mercury simulation software was used to determine the thickness of the layers and Sb content. The thickness of the InAsSb QWs and the AlInAs barriers were found equal to 10 and 17 nm respectively. The Sb content in the wells was determined to be 8.5 % while the Al content in the barrier layers for both samples was 12.2%. These results are in good agreement with the targeted QWs structure characteristics required to obtain emission at 3.4 µm. The full width at half maximum (FWHM) acquired for the AlInAs buffer layer was similar for both samples and roughly equal to162 arcsec.

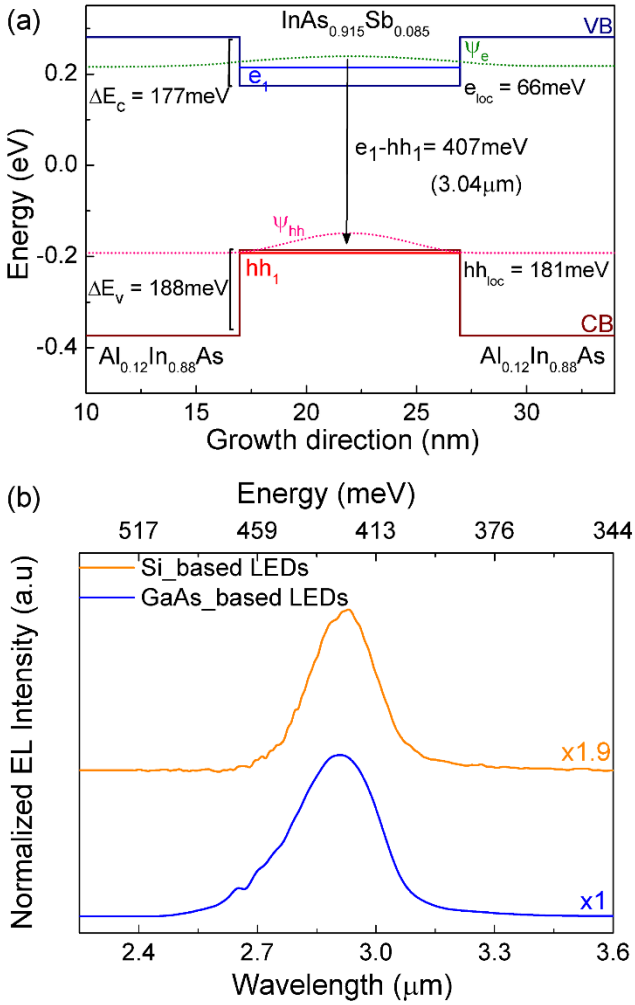

Figure 3: (a) 20 K band diagram simulation of a type-I $InAs_{0.915}Sb_{0.085}/Al_{0.12}In_{0.88}As$ quantum well. The e-hh_1 transition energy, the electron/hole band offsets as well as the localization energies are also shown. (b) 20 K normalised emission spectra measured using 700 mA injection current at 1KHz, 10 % duty cycle for GaAs-based LED (black-line) and Si-based LED (red-line).

Figure 3a shows the band structure of the InAsSb/AlInAs MQWs which was calculated using Nextnano software[18]. A band-gap bowing parameter of 0.65 was used for InAsSb according to previous publications [8,19–22]. The e1-hh1 transition energy was calculated to be 407 meV which is in excellent agreement with the experimental EL peak values, as shown in Figure 3b. The electron and hole localisation energies were determined to be equal to 66 and 181 meV respectively while the electron/hole wavefunction overlap is approximately 80%. The 20K electroluminescence spectra was measured for both InAsSb/AlInAs MQW LEDs operating under the same injection current conditions (700 mA). A single peak emission was observed centred at 426 and 430 meV for the Si and GaAs-based LED respectively, where the spectra

can be interpreted as recombination between the first confined electron state to the ground heavy hole state (e-hh_1). The Si-based LED demonstrated an EL intensity approximately half of that obtained for the GaAs-based LED. This is attributed to the much higher defect density within the active region of the Si-based LED arising from the highly strained InAlAs/GaSb interface.

The temperature dependent electroluminescence spectra measured from the GaAs-based and Si-based MQW LEDs are shown in Figures 4 (a) and (b), respectively. With increasing temperature, the EL spectra of both devices exhibited a red shift, broader linewidth, and

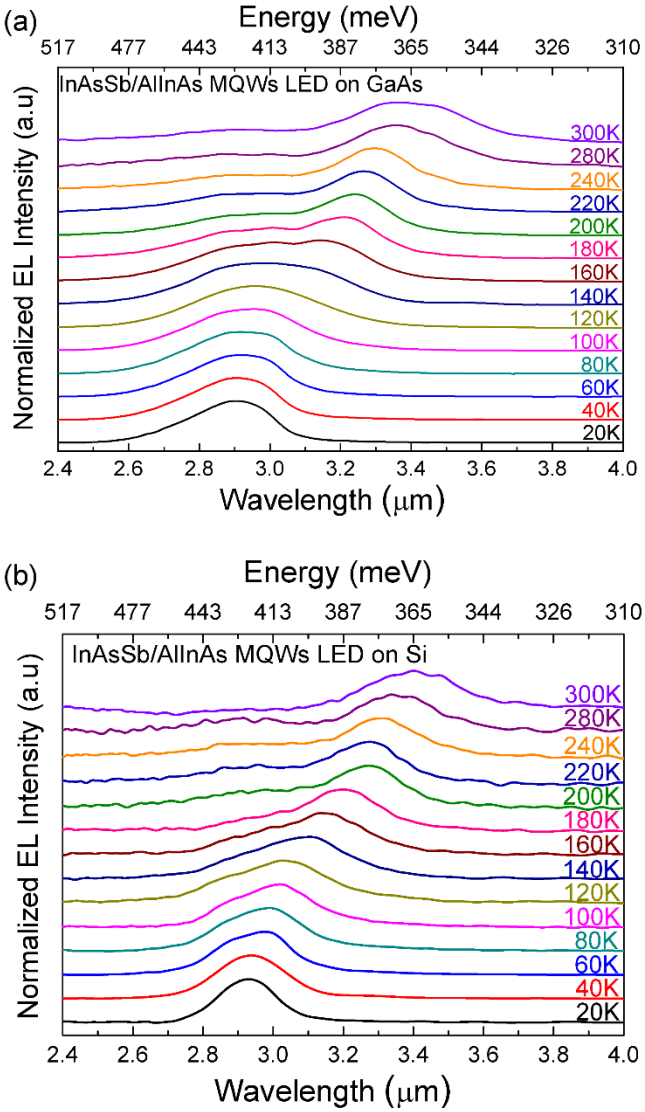

Figure 4: Temperature dependent normalized EL spectra of the (a) GaAs and (b) Si-based LEDs measured using a Bruker Vertex 70 Fourier transform infrared (FTIR) spectrometer. Operating conditions are 700 mA injection current at 1KHz, 10 % duty cycle.

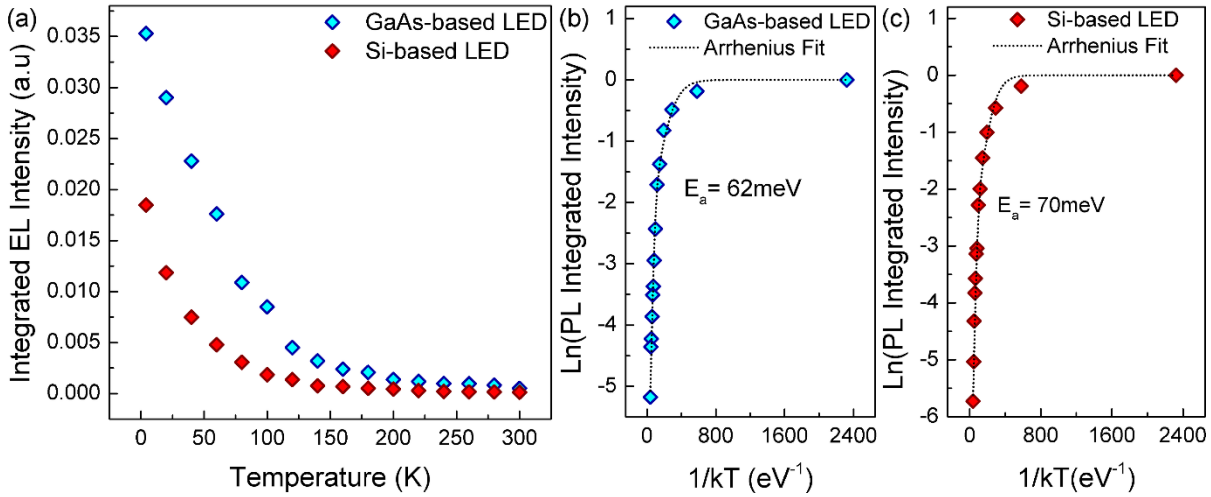

Figure 5: (a) Temperature dependent integrated EL intensity data obtained for both LED devices. (b) and (c) Arrhenius plots of the integrated EL intensity resulting in an activation energy of 62 meV and 70 meV for the GaAs and Si-based LEDs respectively.

significant quenching of the intensity. High energy tails are observed for temperatures higher than 140 K due to the thermalized carrier distribution as carriers at high temperatures occupy sub-band states spreading over a large energy range[15]. The emission spectra are affected by an atmospheric water absorption feature between 2.9 and 3.1 µm. As the emission peak red shifts with increasing temperature, the impact of this absorption is primarily visible in a suppression of the high energy tail. Figure 5a shows the quenching of the EL intensity over the temperature range of 20 to 300 K measured for both Si- and GaAs-based LED. With increasing temperature up to 300 K the integrated intensity decreases by factors of 67 and 136 for the GaAs and Si LED respectively. Figures 5 (b) and (c) show the corresponding Arrhenius plots which were fit using the equation:

$$I = \frac{I_o}{1+C\exp\left(-E_A/K_bT\right)} \qquad (1)$$

where I_o is the EL intensity at temperature T = 0 K, C is the non-radiative process coefficient and E_A is the activation energy of the mechanism responsible for the EL quenching. The dash-dot lines represent the fittings to the experimental data resulting in activation energies of 62 (GaAs) and 70 meV (Si) which are close to the first electron state localization energy (66 meV). This result indicates that leakage of electrons from the QWs is a major mechanism limiting the device performance in addition to the non-radiative Shockley-Read-Hall and Auger recombination. Furthermore, temperature dependence analysis of the EL peak energy of both

LEDs is shown in Figure 6. The measured data were fitted using the Varshni equation [23], which is given by:

$$E_g(T) = E_0 - \alpha T^2/(\beta + T) \quad (2)$$

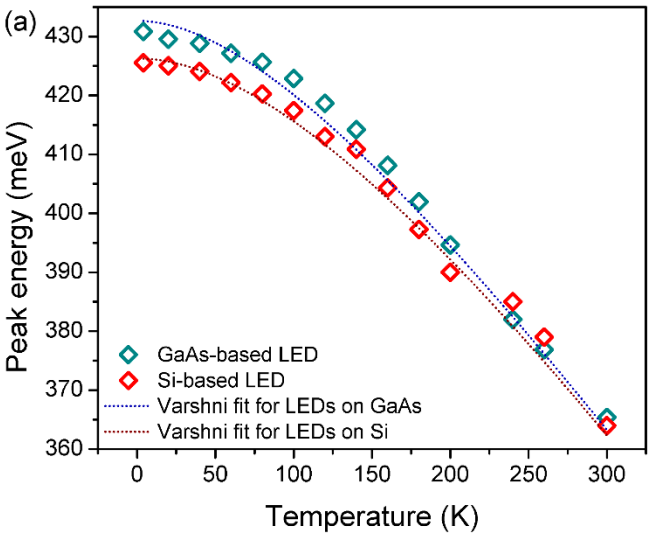

(b)

Structure	Varshni fitting parameters		
	E0 (eV)	α (meV/K)	β (K)
LED on GaAs	0.432	0.39	218
LED on Si	0.426	0.42	300

Figure 6: (a)Temperature dependence of the electroluminescence emission peak energy (e-hh1 transition) obtained for the InAsSb/AlInAs MQW LED integrated on GaAs and Si substrates. The dash-dotted lines represent the Varshni fitting of the experimental data. (b) The Varshni fitting parameters of GaAs and Si-based LED.

where E_0 is the band gap at 0 K, α and β are material dependent constants and T is the temperature in Kelvin. The Varshni fitting parameters given in the table, are in good agreement with those reported previous for bulk InAsSb LEDs grown on Si[16].

Figure 7 shows the output power performance of both LEDs measured at room temperature for different input currents. A low duty cycle of 1% at 1 kHz was used to reduce Joule heating of the devices. Maximum output powers of 63 and 80 μW were obtained at 1500 mA for the GaAs and Si-based LED respectively. The external quantum efficiency of the device can be estimated according to the following:

$$\eta_{ext} = \frac{P\,e}{h\nu\,i} \quad (3)$$

where P is the measured output power, e is electron charge, $h\nu$ is photon energy, and i is the injection current. The external quantum efficiencies were determined to be 0.011 (GaAs) and 0.014% (Si). As shown in Fig. 7, decreasing the input currents below 1A resulted in higher output power values for the GaAs-based LED as compared to that obtained for the Si-based

device in agreement with the low-temperature spectroscopy results. However, for higher currents (>1A), the Si-based LED demonstrated a significantly stronger output power despite the higher defect density. This can be attributed to the improved thermal conductivity of the Si wafer, as reported previously for an Sb-based superlattice LED grown on Si[24].

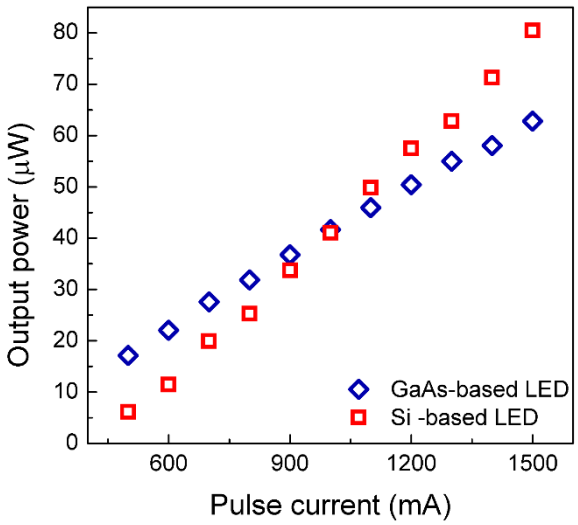

Figure 7: The room temperature output power-current plots obtained for the GaAs and Si-based LEDs at 1KHz using a 1% duty cycle.

4. Conclusion

In summary, MIR InAsSb/AlInAs MQW LED structures were successfully grown on GaAs and silicon wafers operating at around 3.4 um at room temperature. The EL emission spectra were interpreted as recombination between the first confined electron and heavy hole states in the InAsSb QW. Even though the Si-based LED exhibits a higher defect density, the output power measured at room temperature is significantly stronger compared to that obtained for the GaAs-based LED when the injected current is higher than 1A due to the improved thermal conductivity of the substrate. These results suggest that further reduction of the defect density present in the InAsSb/InAlAs MQWs LED integrated onto Si could enable the development of the next-generation, cost-effective sensing and monitoring systems light sources.

Acknowledgements

A.R Altayar was supported by a studentship funded by the ministry of higher education in Saudi Arabia. The authors would like to acknowledge EPSRC [grant number EP/N018605/1] and the Joy Welch Educational Charitable Trust. The data that support the findings of this study

are openly available in [Lancaster University data archive] at http://dx.doi.org/10.17635/lancaster/researchdata/xxx.

References:

[1] Lotsch H K V, Krier A, Huang X L and Sherstnev V V 2006 Mid-infrared Electroluminescence in LEDs Based on InAs and Related Alloys *Mid-infrared Semiconductor Optoelectronics* Springer Series in Optical Sciences vol 118, ed A Krier (London: Springer London) pp 359–94

[2] Hodgkinson J and Tatam R P 2013 Optical gas sensing: a review *Meas. Sci. Technol.* **24** 012004

[3] Jung D, Bank S, Lee M L and Wasserman D 2017 Next-generation mid-infrared sources *J. Opt.* **19** 123001

[4] Parry M K and Krier A 1994 Efficient 3.3 mu m light emitting diodes for detecting methane gas at room temperature *Electron. Lett.* **30** 1968–9

[5] Popov A A, Sherstnev V V, Yakovlev Y P, Baranov A N and Alibert C 1997 Powerful mid-infrared light emitting diodes for pollution monitoring *Electron. Lett.* **33** 86–8

[6] Jung S, Suchalkin S, Kipshidze G, Westerfeld D, Golden E, Snyder D and Belenky G 2010 Dual wavelength GaSb based type I quantum well mid-infrared light emitting diodes *Appl. Phys. Lett.* **96** 191102

[7] Rejeb S B, Debbichi M, Said M, Gassenq A, Tournié E and Christol P 2010 Modelling of an InAs/GaSb/InSb short-period superlattice laser diode for mid-infrared emission by the k.p method *J. Phys. Appl. Phys.* **43** 325102

[8] Keen J A, Lane D, Kesaria M, Marshall A R J and Krier A 2018 InAs/InAsSb type-II strained-layer superlattices for mid-infrared LEDs *J. Phys. Appl. Phys.* **51** 075103

[9] Kurka M, Dyksik M, Suomalainen S, Koivusalo E, Guina M and Motyka M 2019 GaInAsSb/AlGa(In)AsSb type I quantum wells emitting in 3 μm range for application in superluminescent diodes *Opt. Mater.* **91** 274–8

[10] Carrington P J, Solov'ev V A, Zhuang Q, Krier A and Ivanov S V 2008 Room temperature midinfrared electroluminescence from InSb/InAs quantum dot light emitting diodes *Appl. Phys. Lett.* **93** 091101

[11] Muhowski A J, Muellerleile A M, Olesberg J T and Prineas J P 2020 Internal quantum efficiency in 6.1 Å superlattices of 77% for mid-wave infrared emitters *Appl. Phys. Lett.* **117** 061101

[12] Abell J, Kim C S, Bewley W W, Merritt C D, Canedy C L, Vurgaftman I, Meyer J R and Kim M 2014 Mid-infrared interband cascade light emitting devices with milliwatt output powers at room temperature *Appl. Phys. Lett.* **104** 261103

[13] Meyer J R, Bewley W W, Canedy C L, Kim C S, Kim M, Merritt C D and Vurgaftman I 2020 The Interband Cascade Laser *Photonics* **7** 75

[14] Delli E, Hodgson P D, Bentley M, Repiso E, Craig A P, Lu Q, Beanland R, Marshall A R J, Krier A and Carrington P J 2020 Mid-infrared type-II InAs/InAsSb quantum wells integrated on silicon *Appl. Phys. Lett.* **117** 131103

[15] Repiso E, Broderick C A, de la Mata M, Arkani R, Lu Q, Marshall A R J, Molina S I, O'Reilly E P, Carrington P J and Krier A 2019 Optical properties of metamorphic type-I InAs $_{1-x}$ Sb $_{x}$ /Al $_{y}$ In $_{1-y}$ As quantum wells grown on GaAs for the mid-infrared spectral range *J. Phys. Appl. Phys.* **52** 465102

[16] Delli E, Hodgson P D, Repiso E, Craig A P, Hayton J P, Lu Q, Marshall A R J, Krier A and Carrington P J 2019 Heteroepitaxial Integration of Mid-Infrared InAsSb Light Emitting Diodes on Silicon *IEEE Photonics J.* **11** 1–8

[17] Delli E, Letka V, Hodgson P D, Repiso E, Hayton J P, Craig A P, Lu Q, Beanland R, Krier A, Marshall A R J and Carrington P J 2019 Mid-Infrared InAs/InAsSb Superlattice nBn Photodetector Monolithically Integrated onto Silicon *ACS Photonics* **6** 538–44

[18] Birner S, Zibold T, Andlauer T, Kubis T, Sabathil M, Trellakis A and Vogl P 2007 Nextnano: general purpose 3-D simulations *IEEE Trans. Electron Devices* **54** 2137–42

[19] Vurgaftman I, Meyer J R and Ram-Mohan L R 2001 Band parameters for III–V compound semiconductors and their alloys *J. Appl. Phys.* **89** 5815–75

[20] Cripps S A, Hosea T J C, Krier A, Smirnov V, Batty P J, Zhuang Q D, Lin H H, Liu P-W and Tsai G 2007 Midinfrared photoreflectance study of InAs-rich InAsSb and GaInAsPSb indicating negligible bowing for the spin orbit splitting energy *Appl. Phys. Lett.* **90** 172106

[21] Svensson S P, Sarney W L, Donetsky D, Kipshidze G, Lin Y, Shterengas L, Xu Y and Belenky G 2017 Materials design parameters for infrared device applications based on III-V semiconductors *Appl. Opt.* **56** B58

[22] Liu P-W, Tsai G, Lin H H, Krier A, Zhuang Q D and Stone M Photoluminescence and bowing parameters of InAsSb⁄InAs multiple quantum wells grown by molecular beam epitaxy *Appl Phys Lett* 4

[23] O'Donnell K P and Chen X 1991 Temperature dependence of semiconductor band gaps *Appl. Phys. Lett.* **58** 2924–6

[24] Muhowski A J, Bogh C L, Heise R L, Boggess T F and Prineas J P 2019 Improved performance of mid-infrared superlattice light emitting diodes grown epitaxially on silicon *J. Cryst. Growth* **507** 46–9